Preprints.org

Article

Not peer-reviewed version

Analytical Modeling of Eddy Current Loss and Thermal Analysis of Non-Uniform Air Gap Combined Pole Permanent Magnet Motors for Electric Vehicles

Shilun Ma *, Keqi Chen, Changwei Li, Jianwei Ma

Posted Date: 7 May 2024

doi: 10.20944/preprints202405.0341.v1

Keywords: combined pole permanent magnet motor; non-uniform air gap; eddy-current loss; thermal analysis; equivalent thermal network

Preprints.org is a free multidiscipline platform providing preprint service that is dedicated to making early versions of research outputs permanently available and citable. Preprints posted at Preprints.org appear in Web of Science, Crossref, Google Scholar, Scilit, Europe PMC.

Copyright: This is an open access article distributed under the Creative Commons Attribution License which permits unrestricted use, distribution, and reproduction in any medium, provided the original work is properly cited.

Preprints.org (www.preprints.org) | NOT PEER-REVIEWED | Posted: 7 May 2024 doi:10.20944/preprints202405.0341.v1

Disclaimer/Publisher's Note: The statements, opinions, and data contained in all publications are solely those of the individual author(s) and contributor(s) and not of MDPI and/or the editor(s). MDPI and/or the editor(s) disclaim responsibility for any injury to people or property resulting from any ideas, methods, instructions, or products referred to in the content.

Article

Analytical Modeling of Eddy Current Loss and Thermal Analysis of Non-Uniform Air Gap Combined Pole Permanent Magnet Motors for Electric Vehicles

Shilun Ma [1,2,*], Keqi Chen [1], Changwei Li [1] and Jianwei Ma [3]

[1] School of Automobile and Transportation; Tianjin University of Technology and Education; 13187651965@163.com (K.C.); LiChangwei32@163.com (C.L.)
[2] Tianjin Zhenghan Technology Co., LTD, Tianjin 300222, China; majianwei01@xpc.edu.cn (J.M.)
[3] Hebei Vocational University of Technology and Engineering
* Correspondence: 18698008183@163.com; Tel.: +86-18698008183

Abstract: In order to solve the problem of large eddy current loss and high temperature rise caused by large amount of permanent magnet, a new type of combined magnetic pole permanent magnet motor is proposed in this paper. The sinusoidal distribution subdomain model of non-uniform air gap rotor is established by using Laplace equation, and the analytical expression of eddy current loss of rotor in uniform air-gap and non-uniform air-gap is derived. The effect of rotor eccentricity on eddy current loss is obtained. According to the characteristics of distributed winding of non-uniform air gap combined pole permanent magnet motor, equivalent treatment is performed to obtain the equivalent thermal conductivity, so as to establish equivalent thermal network model of motor, calculate the temperature value of each component of the motor, and verify the correctness of the thermal network model through the method of magnetothermal bidirectional coupling. Finally, an experimental platform is set up to carry out temperature rise experiments on the two prototypes respectively. Experimental results show that the non-uniform air-gap rotor structure can effectively reduce the rotor eddy current loss and motor temperature rise, and also verify the accuracy of the analytical model calculation results.

Keywords: combined pole permanent magnet motor; non-uniform air gap; eddy-current loss; thermal analysis; equivalent thermal network

Introduction

In order to solve the energy crisis and environmental pollution problems caused by internal combustion engine vehicles, automobile companies and research institutes in various countries have taken energy conservation and emission reduction as the main development plan of future vehicles [1-2], Due to electric vehicles have the characteristics of low pollution, zero emission, high energy efficiency and diversified energy sources, the development of various new energy vehicles represented by electric vehicles has become an effective way to solve many problems caused by traditional fuel vehicles [3]. Electric drive system is the key assembly of electric vehicle, and its performance directly affects the power and economy of electric vehicle. Compared with switched reluctance motor, induction motor and brushless DC motor, permanent magnet synchronous motor has the advantages of high power density, high overload capacity and high efficiency, and has been widely used in electric vehicle power drive system. However, for the permanent magnet motor, the magnetic energy generated by the permanent magnet and the stator tooth slot will produce a tooth slot effect, resulting in a large harmonic content in the motor magnetic field, which will produce a large number of eddy current loss and harmonic loss on the fixed rotor and permanent magnet. The loss is the heat source, and the loss will cause the internal temperature of the motor to rise in the form of heat [4-5]. In addition, since the armature winding of the permanent magnet motor needs to be

© 2024 by the author(s). Distributed under a Creative Commons CC BY license.

Preprints.org (www.preprints.org) | NOT PEER-REVIEWED | Posted: 7 May 2024 doi:10.20944/preprints202405.0341.v1

embedded in the stator slot, the heat source is relatively concentrated, which will cause the motor heat dissipation difficulties when the heat increase. Too high temperature rise of the permanent magnet motor will cause the performance of the magnetic material to be reduced, and even lead to irreversible demagnetization of the permanent magnet. Therefore, accurate analysis of the temperature rise distribution of the permanent magnet motor can reduce the heat output. It is very important to improve the power density of electric vehicle drive system.

In recent years, many researchers at home and abroad have done a lot of research on the calculation methods and influencing factors of motor temperature rise. Literature [5] analyzed the two-dimensional temperature field of motor, ignoring the distribution and change of the motor along the axis. Literature [6] used equivalent thermal network method and finite element method respectively to calculate the stable temperature rise and transient temperature rise of an electric vehicle motor under rated working conditions, and verified the adaptability and compatibility of the two methods. In literature [7], the effect of rotor pole optimization on the loss and temperature rise of interior permanent magnet synchronous motor was studied, and then verified by finite element magnetic thermal coupling analysis. However, the processing cost of irregular permanent magnet is high. Literature [8] and [9], the method of permanent magnet segment is adopted to reduce eddy current loss and lower temperature rise. In addition, there are some literatures using the method of unequal turn winding and stator yoke setting magnetic bridge to reduce eddy current loss and motor temperature rise, but these methods will make the motor manufacturing process complicated [10-11]. In Lterature [12], the double three phase winding is used to suppress the high harmonic content in the armature field of 10 poles and 12 slots permanent magnet motor, and the motor structure is more complicated and the reliability is reduced. Literature [13] proposed a three-dimensional numerical hybrid calculation method based on the combination of static three-dimensional finite element method and three-dimensional finite difference method. The calculation accuracy of this method is relatively high, but the modeling is relatively complex and requires finite element pre-processing. Meanwhile, this method can only consider the eddy current loss of rectangular permanent magnet, and its flexibility is also limited to a certain extent. Literature [14] studies the effects of surface slot depth, slot mode and number of slot on eddy current loss of permanent magnets, the results show that the slot depth is related to the penetration depth of higher harmonics, and too deep slot not only can not further restrain eddy current loss, but also will reduce the rotor strength. To sum up, most of the existing literature focuses on the loss and thermal analysis of traditional interior single-pole permanent magnet motors, while few literatures focus on the thermal analysis of interior combined magnetic pole permanent magnet motors. In addition, current literature is conducted on the basis of uniform air gap, and no relevant literature has been found to explore the influence of non-uniform air gap on eddy current loss and temperature rise.

This paper introduces the structure and magnetic circuit characteristics of interior combined pole permanent magnet motor, analyzes the electromagnetic characteristics of the non-uniform air gap permanent magnet motor and the mechanism of eddy current loss. By establishing the sinusoidal distribution subdomain model of the non-uniform air gap, and using Fourier decomposition method and Laplace equation, the analytical expression of the eddy current loss of the motor is derived, so as to obtain the eddy current loss under different rotor eccentricity. The principle of low eddy current loss of permanent magnet motor with non-uniform air gap rotor structure is described. The equivalent thermal network model of the motor is established and three-dimensional unidirectional and bi-directional magneto thermal coupling finite element models of the motor are established respectively. The loss was accurately transferred to each part of the motor for thermal analysis, and the motor temperature rise of different analysis methods is compared. Two prototype is produced and experimental platform is set up for testing. The research work in this paper provides a reference method for loss analysis and temperature rise analysis of interior permanent magnet motors.

1. Structural Parameters of Permanent Magnet Motor

The interior tangential and double-radial permanent magnet motor (ITRPMM) proposed in this paper is shown in Figure 1. Each magnetic pole on the rotor structure is composed of tangential

Preprints.org (www.preprints.org) | NOT PEER-REVIEWED | Posted: 7 May 2024 doi:10.20944/preprints202405.0341.v1

magnetic field rectangular permanent magnet (TRPM), radial magnetic field rectangular permanent magnet (RRPM) and semi-circular radial magnetic field permanent magnet (SRPM).

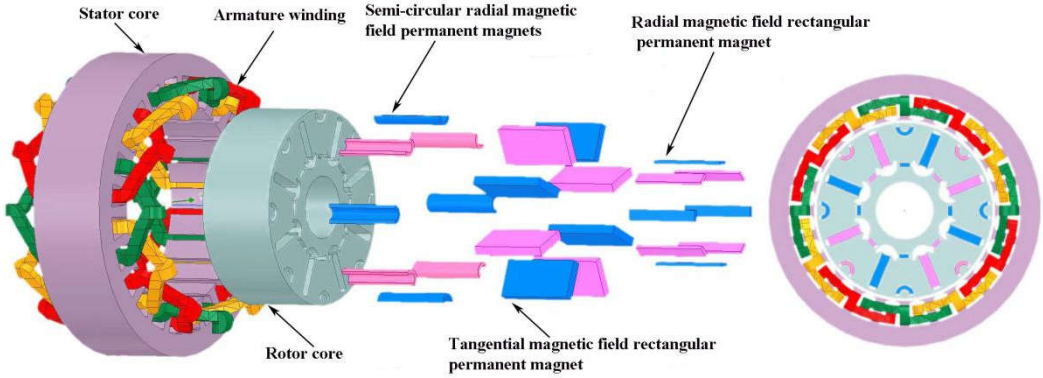

Figure 1. The structure diagram of ITRPMM. 1. Stator core; 2. Armature winding; 3. semi-circular radial magnetic field permanent magnet（SRPM）; 4. Radial magnetic field rectangular permanent magnet （RRPM）; 5. Rotor core; 6. Tangential magnetic field rectangular permanent magnet (TRPM).

According to the performance requirements of permanent magnet motor for electric vehicles, the structural parameters of ITRPMM are determined by empirical formula, as shown in Table 1. The structure diagram of ITRPMM, as shown in Figure 1.

Table 1. Structural parameter ofers of new type of permanent magnet motor.

Parameters	Values	Parameters	Values
Rated voltage /V	60	Rated speed /r·min	3000
Rated power/kW	3	Outer diameter of rotor /mm	89
Number of pole pairs	4	Interior diameter of rotor /mm	30
Slots	36	Axial length /mm	60
Inner diameter of stator /mm	90	Number of turns per slot	11
Outer diameter of stator /mm	145	Volume of permanent magnet /mm^3	72000

2. Establishment of Subdomain Model of Sinusoidal Distribution of Non-Uniform Air Gap

At present, the research of permanent magnet motor by experts and scholars at home and abroad is based on the fixed rotor axis coincidence (that is, uniform air gap). The rotor shape of the uniform air gap structure is a standard circle, and the outer circle of the rotor and the rotating shaft are centered at point o. In order to study the influence of non-uniform air gap on the output characteristics of the motor, a non-uniform air gap motor model is established, as shown in Figure 2, the rotor outer circle is composed of 8 arc segments with different centers from the outer circle of stator; Rotor eccentricity $H=oo'$, the size of which can be used to measure the eccentricity of non-uniform air gap.

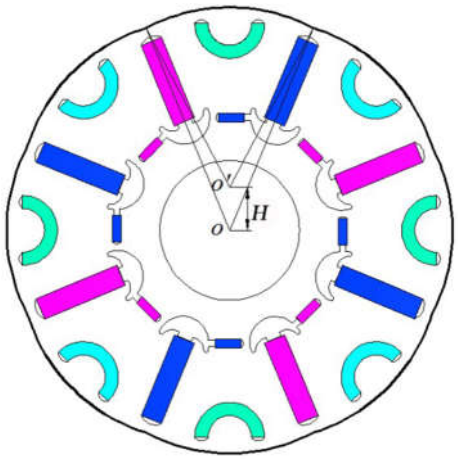

Preprints.org (www.preprints.org) | NOT PEER-REVIEWED | Posted: 7 May 2024 doi:10.20944/preprints202405.0341.v1

Figure 2. Rotor structure with non-uniform air gap.

According to the geometric relationship, the formula of rotor eccentricity varying with air gap length is derived:

$$H = \sqrt{(R_1 - \delta)^2 + 2\delta R_2 \cos\alpha - R_2^2} \tag{1}$$

where, R1 is inner diameter of stator; R2 is outer diameter of rator; δ is length of air gap; α is circumference Angle of motor;

When motor is unloaded, the current in the armature winding is 0, and air gap magnetic field is irrotational field. In this case, the scalar magnetic potential satisfies the Laplace equation, and a rectangular coordinate system can be established to solve the problem, as shown in Figure 3. where, Bg is air gap flux density, and permeability of the stator core and the rotor core is μ_{Fe} .

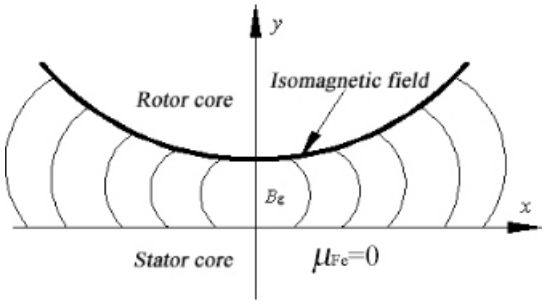

Figure 3. The distribution of air gap when magnetic field is sinusoidal.

In two-dimensional rectangular coordinate system, Laplace's equation is used to solve the scalar magnetic potential equation:

$$\Omega = \sum_{k=1}^{\infty} (A_k \cos m_k x + B_k \sin m_k x)(C_k \mathrm{sh} m_k y + D_k \mathrm{ch} m_k y) \tag{2}$$

where, Ω is magnetic bit; A_k, B_k, C_k, D_k, m_k are constants determined by the boundary conditions.

Assuming $\mu_{Fe} = \infty$,the boundary conditions can be expressed

$$\text{When } y = 0,\ \Omega = 0 \tag{3}$$

$$\text{When } y = \delta,\ \Omega = \Omega_0 \tag{4}$$

Assuming that the surface magnetic field of the stator core is sinusoidal, when y = 0, it can be obtained

$$B_y = -B_g \cos\frac{\pi}{\tau} x \tag{5}$$

where, By is the magnetic density component of the air gap along the y axis; τ is polar distance of rotor

By substituting formula (3) into formula (2), can be deduced

$$\sum_{k=1}^{\infty} (A_k \cos m_k x + B_K \sin m_k x) D_k = 0 \tag{6}$$

According to formula (6),$D_k = 0$ is obtained. Therefore, formula (2) becomes

$$\Omega = \sum_{k=1}^{\infty} (A_k' \cos m_k x + B_K' \sin m_k x) \mathrm{sh}\, m_k y \tag{7}$$

where, $A_k' = \dfrac{B_g}{\mu_0 m_k}; m_k = \dfrac{\pi}{\tau}; B_k' = 0$.

Preprints.org (www.preprints.org) | NOT PEER-REVIEWED | Posted: 7 May 2024 doi:10.20944/preprints202405.0341.v1

According to the second formula of the boundary conditions, that is, equation (4), the magnetic density of the air gap at y = 0 can be obtained

$$B_{y(y=0)} = -B_g \cos\frac{\pi}{\tau}x \tag{8}$$

By substituting formula (8) into formula (7), obtained

$$\Omega = \frac{B_g \tau}{\mu_0 \pi}\cos\frac{\pi}{\tau}x\,\mathrm{sh}\frac{\pi}{\tau}y \tag{9}$$

Using formula (4), the magnetic potential at y = δ on the surface of the rotor core can be obtained

$$\Omega = \frac{B_g \tau}{\mu_0 \pi}\cos\frac{\pi}{\tau}x\,\mathrm{sh}\frac{\pi}{\tau}\delta \tag{10}$$

When the central position of the rotor core x = 0, y = δ0, can be obtained

$$\Omega = \frac{B_g \tau}{\mu_0 \pi}\cos\frac{\pi}{\tau}x\,\mathrm{sh}\frac{\pi}{\tau}\delta_0 \tag{11}$$

Divide equation (10) and equation (11) to obtain

$$\mathrm{sh}\frac{\pi}{\tau}\delta = \frac{\mathrm{sh}\frac{\pi}{\tau}\delta_0}{\cos\frac{\pi}{\tau}x} \tag{12}$$

After sorting out the formula (12), the expression of non-uniform air gap length can be obtained.

$$\delta = \frac{\tau}{\pi}\mathrm{sh}^{-1}\left(\frac{\mathrm{sh}\frac{\pi}{\tau}\delta_0}{\cos\frac{\pi}{\tau}x}\right) \tag{13}$$

By substituting formula (13) into formula (1), the relationship between non-uniform air gap and rotor eccentricity can be expressed

$$\delta = \frac{(R_1^2 - R_2^2) - H^2}{2R_1 + 2R_2\cos\alpha + \frac{\iota}{\pi}sh^{-1}\left(\frac{sh\frac{\pi}{\iota}\delta_0}{\cos\frac{\pi}{\iota}}\right)} \tag{14}$$

3. Establishment of Analytical Model of Eddy Current Loss of Rotor Core

At present, the core of the permanent magnet rotor is mostly made of silicon steel sheet laminated. It is assumed that the eddy current loss of the rotor core exists only in each silicon steel sheet. Eddy current loss model of silicon steel sheet was established, as shown in Figure 4.

Preprints.org (www.preprints.org) | NOT PEER-REVIEWED | Posted: 7 May 2024 doi:10.20944/preprints202405.0341.v1

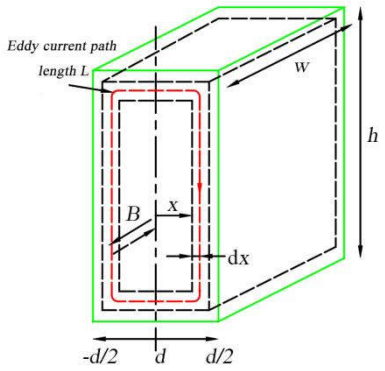

Figure 4. Eddy current loss model of silicon steel sheet.

When the magnetic flux density B passes through the silicon steel sheet with resistivity ρ in the arrow direction in Figure 4, the eddy current loss P_E generated by the silicon steel sheet can be calculated as

$$P_E = \int_0^{\frac{d}{2}} dP_E = \frac{w}{2}\int_0^{\frac{d}{2}} E^2 dx \tag{15}$$

where, dP_E is the differential of eddy current loss at a given power, E is the effective value of inductance voltage on eddy current flux circuit, which can be calculated as

$$E = 2\pi f \bullet B\sqrt{2}h \tag{16}$$

where, f is motor frequency.

By substituting formula (16) into (15), obtained.

$$P_{Fe} = \frac{V\pi^2 f^2 d^2 B^2}{6\rho} \tag{17}$$

where, V is the volume of the silicon steel sheet, $V = d \cdot w \cdot h$.

When the main performance indicators of the permanent magnet motor are determined, the above parameters are basically determined. Therefore, to reduce the rotor eddy current loss, it is necessary to start from the magnetic flux density B of rotor core into the silicon steel sheet. Due to the different magnetic flux density of rotor core at different positions, it is difficult to determine. In this paper, the relation between the main air gap magnetic flux density B_r and rotor core magnetic flux density B can be expressed.

$$B_r = \sigma \bullet B \tag{18}$$

where, σ is the magnetic leakage coefficient of the rotor magnetic field.

The main air gap flux density B_r distributed radially along the rotor surface can be calculated:

$$B_r = F(x) \bullet \lambda(x) \tag{19}$$

where, $F(x)$ is magnetomotive force of magnetic field of rotor in air gap; $\lambda(x)$ is permeability of air gap distributed radially along rotor surface.

By Fourier decomposition of $F(x)$ and $\lambda(x)$ respectively, the expression of the magnetic density of the main air gap after Fourier transform can be obtained as follows:

$$\begin{aligned} B(\theta,t) &= F_v(\theta,t) \bullet \lambda(\theta,t) \\ &= \sum_v \frac{f_v}{k_g}\Lambda_0 \cos(v\theta - \omega t) + \sum_{v_z} \frac{f_0}{k_g}\Lambda_k \cos(v_z\theta - \omega t) + \sum_{v_z} k_g \frac{f_v}{2}\Lambda_k \cos(v_z\theta - \omega t) \end{aligned} \tag{20}$$

where, $F_v(\theta,t)$ is magnetomotive force in main air gap after Fourier decomposition; $\lambda(\theta,t)$ is permeability of air gap after Fourier decomposition; f_v is the harmonic amplitude of stator

Preprints.org (www.preprints.org) | NOT PEER-REVIEWED | Posted: 7 May 2024 doi:10.20944/preprints202405.0341.v1

magnetomotive force. k_g is magnetic saturation coefficient of motor; Λ_0 is Invariant part of air gap magnetic permeability, $\Lambda_0 = \frac{\mu_0}{\delta K_c}$ ； K_c is Carter coefficient, $K_c = \frac{t}{t-\gamma\delta}$, γ is coefficient; f_0 is fundamental amplitude of magnetomotive force; v is number of harmonic poles of the stator magnetomotive force; v_z is the number of harmonic poles of stator teeth; ω is rotational angular velocity of fundamental wave of stator magnetomotive force; Λ_k is harmonic amplitude of rotor surface air gap permeability.

It can be obtained by sorting out formula (20) :

$$\begin{aligned} B_r &= \sum_v \frac{f_v}{k_g}\Lambda_0 \cos(v\theta-\omega t) + \sum_{v_z}\frac{f_0}{k_g}\Lambda_k\cos(v_z\theta-\omega t) + \sum_{v_z} k_g\frac{f_v}{2}\Lambda_k\cos(v_z\theta-\omega t) \\ &= \sum_v \frac{f_v}{k_g}\bullet\frac{\mu_0(t-\gamma\delta)}{\delta t}\cos(v\theta-\omega t)+C \end{aligned} \tag{21}$$

where， $C = \sum_{v_z}\frac{f_0}{k_g}\Lambda_k\cos(v_z\theta-\omega t) + \sum_{v_z} k_g\frac{f_v}{2}\Lambda_k\cos(v_z\theta-\omega t)$;

By substituting equations (20) and (14) into (16), the relation between eddy current loss and rotor eccentricity can be obtained:

$$\begin{aligned} P_{Fe} &= \frac{V\pi^2 f^2 d^2\left[\sum_v \frac{f_v}{k_g}\bullet\frac{\mu_0(t-\gamma\delta)}{\delta t}\cos(v\theta-\omega t)+C\right]^2}{6\rho\sigma^2} \\ &= \frac{V\pi^2 f^2 d^2\left[\sum_v \frac{f_v}{k_g}\bullet\frac{\mu_0[t-\gamma\frac{(R_1^2-R_2^2)-H^2}{2R_1+2R_2\cos\alpha+\frac{\iota}{\pi}sh^{-1}(sh\frac{\pi}{\iota})(\cos\frac{\pi}{\iota})^{-1}}]}{t\bullet[(R_1^2-R_2^2)-h^2]}\cos(v\theta-\omega t)+C\right]^2}{6\rho\sigma^2} \end{aligned} \tag{22}$$

The eddy current losses of permanent magnet motors with uniform and non-uniform air gaps were calculated by finite element method and model analysis method respectively, as shown in Figure 5. It can be seen that with the increase of rotor eccentricity, peak value of eddy current loss does not increase or decrease linearly, but approaches to aparabola, and When the rotor eccentricity is 4mm, the minimum eddy current loss occurs at 27W. The results of finite element analysis are in good agreement with analytical calculation, which verifies the correctness of eddy current loss model of non-uniform air gap combined pole permanent magnet motor.

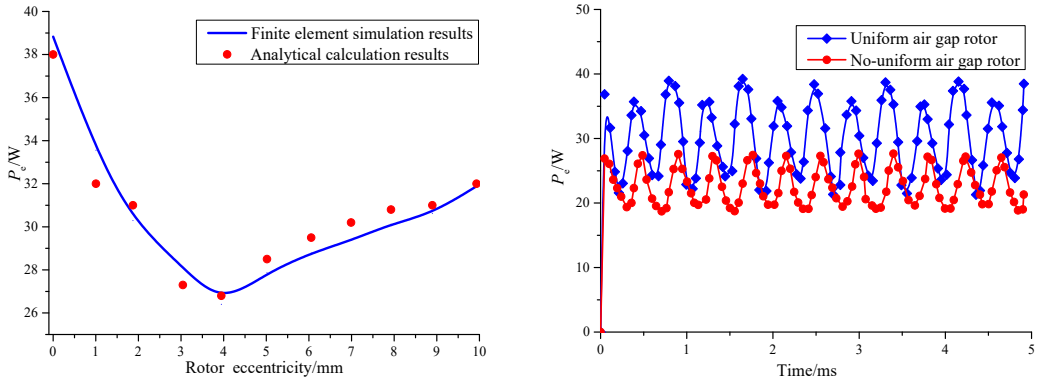

(a)The relationship between eddy current loss and rotor eccentricity

(b) Finite element simulation results with and without rotor eccentricity

Figure 5. The influence of rotor eccentricity on eddy current losses.

Preprints.org (www.preprints.org) | NOT PEER-REVIEWED | Posted: 7 May 2024 doi:10.20944/preprints202405.0341.v1

4. Establishment of Equivalent Thermal Network Model

4.1. Equivalent Thermal Network Model

In the process of designing permanent magnet drive motor, the internal temperature field defense of the motor and the influence of external heat dissipation on each part of the motor is a problem that cannot be ignored. Because there are many factors affecting the temperature rise of the motor, and they directly affect the accuracy of the temperature rise meter of the motor, on the basis of thermal path analysis, The equivalent thermal network method, which uses network topology as a calculation tool to model and analyze the temperature of the motor locally and as a whole, is widely used in practice due to its simple calculation process [15-16].

In order to facilitate the establishment of an equivalent thermal network for solving, the following assumptions were made before establishing the model: (1) ignoring the skin effect of the winding in the stator slot of the motor; (2) the distribution of heat sources inside the motor is uniform, and the stray losses of the motor are concentrated in the stator teeth; (3) the heat inside the motor is only exchanged through thermal conduction and convection, ignoring the influence of thermal radiation.

The shape of each part of motor is mainly composed of cylindrical and cuboid, such as the heat fin on the shell, radial and tangential permanent magnet steel is rectangular, while the semi-circular permanent magnet, fixed rotor core, motor shell can be regarded as cylindrical, and the thermal conductivity and thermal resistance of the motor parts can be obtained by the following equation.

Thermal resistance equation of cuboid components:

$$R_{\mathrm{j}} = \frac{L_{\mathrm{c}}}{\lambda_{\mathrm{j}} S_{\mathrm{j}}} \tag{23}$$

where, L_{c} is the heat transfer length of the cuboid component; S_{j} is the contact area of cuboid components; a is the thermal conductivity of cuboid material.

Thermal resistance equation of cylindrical component.

$$R_y = \frac{L_y}{\lambda_{\mathrm{T}} S_{\mathrm{dx}}} = \frac{\ln(\frac{r_w}{r_n})}{2\lambda_{\mathrm{T}}\pi} \tag{24}$$

where, R_y is radial thermal conductivity resistance of cylindrical components; r_{w} is outer radius of cylindrical component; r_n is the inner radius of the cylinder component; S_{dx} is the contact area or equivalent heat dissipation area between the component and the cooling fluid; λ_{T} is thermal conductivity of cylindrical component.

According to the above thermal conductivity and thermal resistance modeling theorem, the nodes of ITRPMM are divided, and the circumferential half of the motor is dissected and analyzed because the motor is symmetrical. Figure 6 shows the simplified equivalent thermal network calculation model.

Preprints.org (www.preprints.org) | NOT PEER-REVIEWED | Posted: 7 May 2024 doi:10.20944/preprints202405.0341.v1

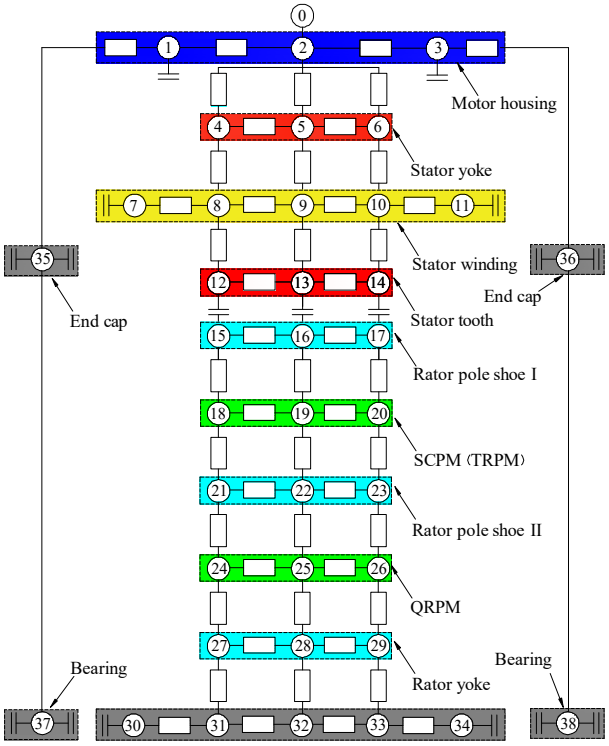

Figure 6. Equivalent thermal network model of motor.

As can be seen in Figure. 6, the materials of each component of the motor are used as the influencing factors to divide the motor into regions, and a total of 38 calculation regions are divided into nodes at each position to simulate the real state of the heat conduction path, with node 0 as the external environment node, nodes 1-3 as the motor casing nodes, nodes 4-6 as the stator yoke nodes, nodes 7-11 as the stator winding nodes, nodes 12-14 as the stator tooth nodes, nodes 15-17 as the rotor frontal nodes, nodes 18-20 as the semicircular or tangential rectangular permanent magnet nodes, nodes 21-23 as the rotor between the radial rectangular magnet and the semicircular permanent magnet Nodes 15-17 are rotor frontal nodes, nodes 18-20 are nodes of semicircular or tangential rectangular permanent magnets, nodes 21-23 are nodes of rotor core between radial rectangular magnets and semicircular permanent magnets, nodes 24-26 are nodes of radial rectangular permanent magnets, nodes 27-19 are nodes of rotor core with radial permanent magnets, nodes 30-34 are nodes of rotor shaft, nodes 35-36 are nodes of front and rear air cavities of the motor and nodes 37 are nodes of main air gap. 37 are the main air gap nodes.

4.2. Equivalent Model of Armature Winding

Usually in the motor in the armature winding wires in the slot arrangement is irregular, the insulation material distribution is not uniform, as shown in Figure 7 (a), so part of the heat in the stator slot in the transfer, the direction of heat transfer can not be accurately obtained. In order to simplify the calculation, the thermal field model of the stator slot can be equated as follows: all the copper wires in the slot, the insulating film and the residual air gap between the wires are regarded as a heat conductor, and the slot insulation is regarded as another heat conductor for the calculation, and the armature winding after equating is shown in Figure 7(b).

Preprints.org (www.preprints.org) | NOT PEER-REVIEWED | Posted: 7 May 2024 doi:10.20944/preprints202405.0341.v1

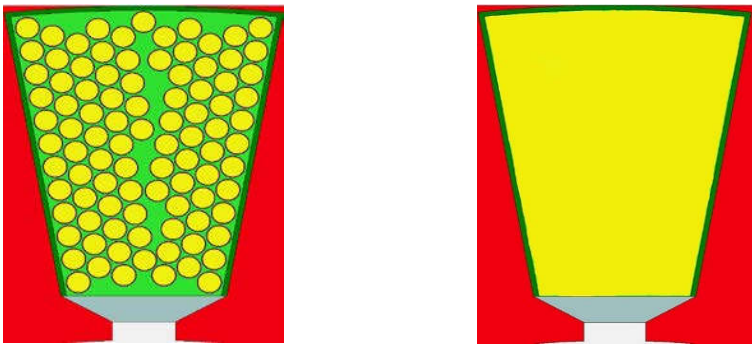

(a) Intial model of stator winding (b) Equivalent model of stator winding

Figure 7. Equivalent model of armature winding.

The thicknesses of the copper wires, insulating varnish and insulating paper in the different heat transfer directions are different and converted. According to the slot width and depth. the equivalent thermal coefficient of the armature winding in the stator slot along the axial direction can be calculated using equation (25):

$$\lambda_{xi} = \sum_{i=1}^{n} l_x \Big/ (\sum_{x=1}^{n} \frac{l_x}{\lambda_{xi}}) \tag{25}$$

where, l_x is thickness of copper wire and insulating paper along the x direction; λ_{xi} is the thermal conductivity of copper wire and insulating paper.

Equivalent thermal conductivity of the armature winding in the stator slot along the radial direction can be calculated using equation (26):

$$\lambda_{yi} = \sum_{y=1}^{n} l_y \Big/ (\sum_{y=1}^{n} \frac{l_y}{\lambda_{yi}}) \tag{26}$$

where, l_y is thickness of copper wire and insulating paper along the y direction; λ_{yi} is the thermal conductivity of copper wire and insulating paper.

4.3. Calculation Results of the Equivalent Thermal Network Model

According to the principle of heat balance, it can be seen that the heat generated by each unit of the motor and the incoming heat should be equal to the heat output from the unit in the steady state condition. The heat balance equations for the equivalent network nodes of ITRPMM can be listed with the matrix expression:

$$|\Delta G| \bullet |\Delta T| = |\Delta P| \tag{27}$$

where, $|\Delta G|$ is the thermal conductivity matrix; $|\Delta T|$ is the node temperature matrix; $|\Delta P|$ is the heat source matrix.

Assuming that the external ambient temperature is 25℃ at room temperature, according to the above determined heat dissipation conditions of the motor, the temperature rise of the permanent magnet motor is calculated using the established equivalent thermal network model, so as to obtain the temperature rise of each node inside the permanent magnet drive motor, and each component is averaged to ultimately obtain the results of solving the temperature rise of each component of the permanent magnet motor.

5. Magneto-Thermal Bi-Directional Coupling Finite Element Simulation Analysis

The problem of loss and temperature rise of permanent magnet motor is a coupled problem. The magnitude of loss will cause the change of temperature rise, and the temperature rise of the motor will affect the permanent magnet remanent magnetism and coercivity, which in turn affects the loss

Preprints.org (www.preprints.org) | NOT PEER-REVIEWED | Posted: 7 May 2024 doi:10.20944/preprints202405.0341.v1

of the motor. For permanent magnet motors applied to electric vehicles, the rated thermal load is higher during load operation, and when the temperature exceeds the demagnetization temperature of the permanent magnet, irreversible demagnetization occurs, which will reduce the service life of the permanent magnet drive motors, Therefore the accurate calculation of the temperature field will directly affect the reliability of motor.

By using equivalent thermal network to analyze the motor, the model can be simplified and solved quickly. Although the calculation speed is fast, the equivalent thermal network method can not directly obtain the temperature distribution of each part of the motor. If the component is more complex, the equivalent thermal network method is difficult to solve and the precision is not high. In order to carry out further thermal analysis of the motor and verify the calculation results of the equivalent thermal network, magnetothermal coupling simulation of the motor is carried out. In order to improve the accuracy of calculation, three-dimensional field is used in the electromagnetic characteristic analysis and thermodynamic simulation of the motor. The three-dimensional diagram of ITRPMM is shown in Figure 8.

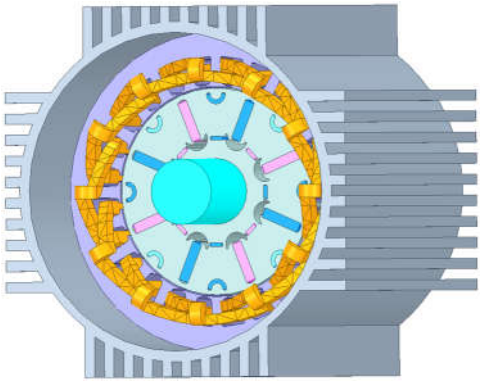

Figure 8. The three-dimensional diagram of ITRPMM.

The use of magneto-thermal coupling finite element analysis can save the simulation time, while having a better computational accuracy. Generally, there are two schemes for the coupling of the electromagnetic field and the temperature field, unidirectional coupling and bidirectional coupling[17-18] . In unidirectional coupling, the electromagnetic field calculation and the temperature field calculation are carried out separately, and the results of the electromagnetic field are directly used in the calculation of the temperature field. The bi-directional coupling is through the mutual transfer of data to make the electromagnetic field analysis and temperature field analysis at the same time, in the magnetic field analysis to calculate the loss as the heat source of the temperature field, in the temperature field analysis to calculate the temperature used to determine the electromagnetic field analysis of the material properties, the formation of closed-loop transmission of the data, and so on for many iterations of the calculation until the temperature reaches the set error range or reaches the maximum number of iterations. In order to calculate the temperature field of the motor more accurately, the two-way coupling method is used to study it, and the magneto-thermal bi-directional coupling model is schematically shown in Figure 9.

Preprints.org (www.preprints.org) | NOT PEER-REVIEWED | Posted: 7 May 2024 doi:10.20944/preprints202405.0341.v1

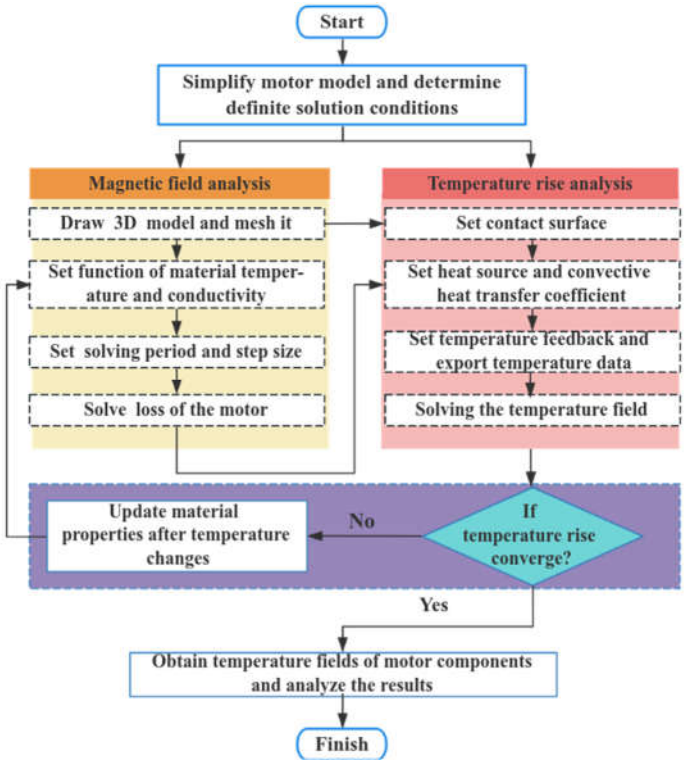

Figure 9. Flow chart of magneto-thermal bi-directional coupling.

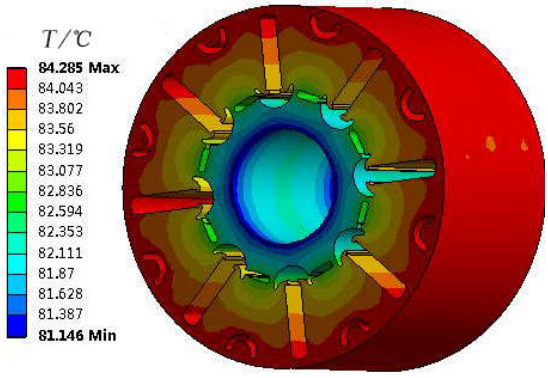

(a) Temperature rise of rotor core

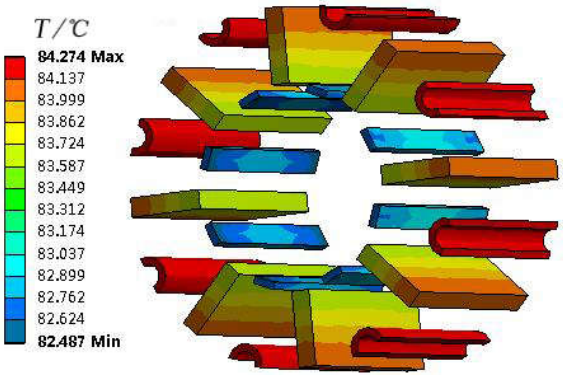

(b) Temperature rise of permanent magnet

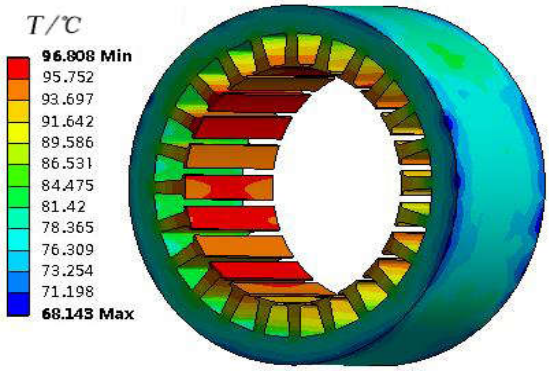

(c) Temperature rise of stator core

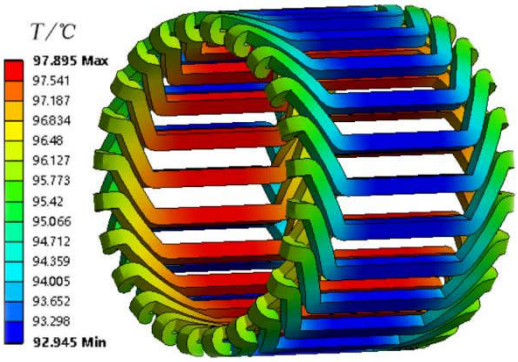

(d) Temperature rise of armature winding

Preprints.org (www.preprints.org) | NOT PEER-REVIEWED | Posted: 7 May 2024 doi:10.20944/preprints202405.0341.v1

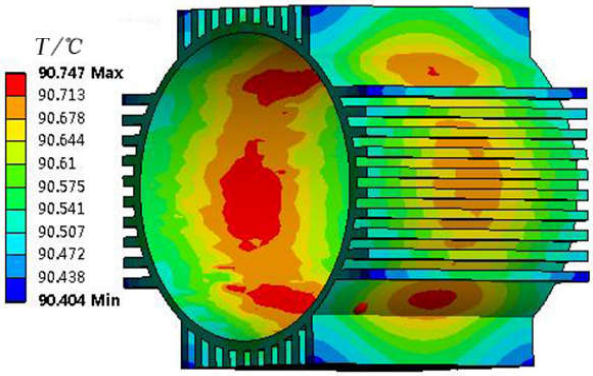

(e) Temperature rise of motor housing

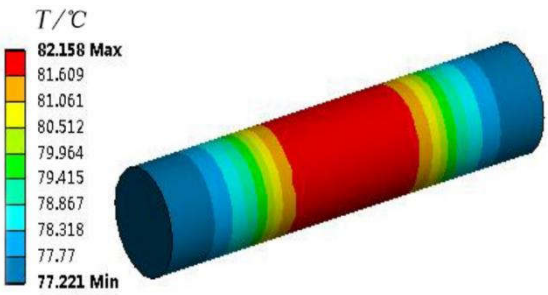

(f) Temperature rise of shaft

Figure 10. Temperature rise of each part of motor with uniform air gap structure at rated load for 120 min of operation.

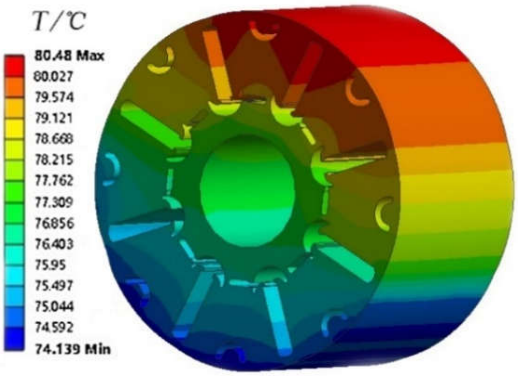

(a) Temperature rise of rotor core

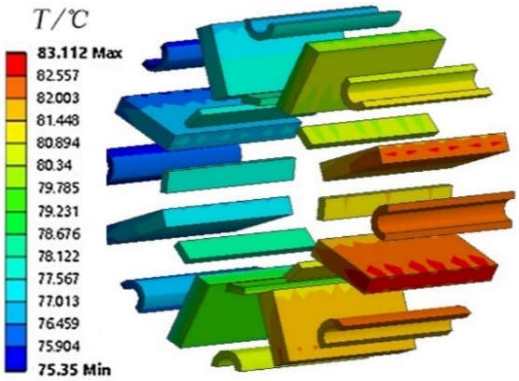

(b) Temperature rise of permanent magnet

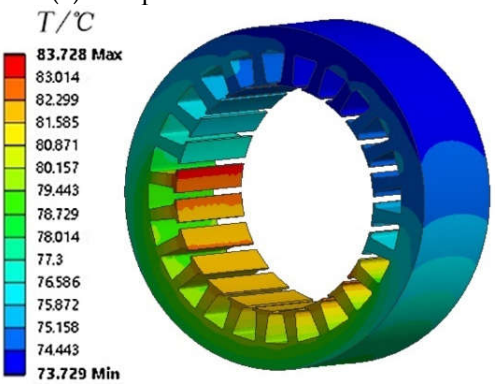

(c) Temperature rise of stator core

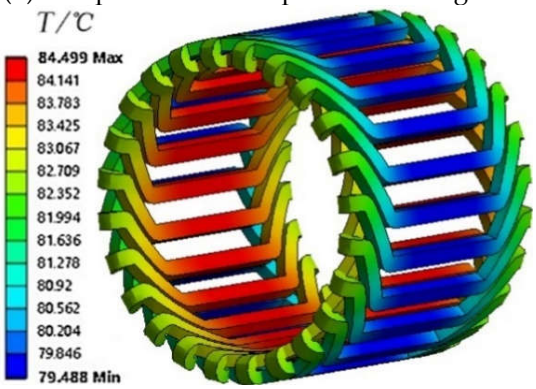

(d) Temperature rise of armature winding

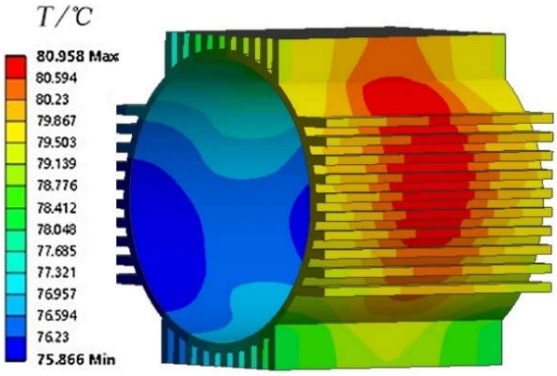

(e) Temperature rise of motor housing

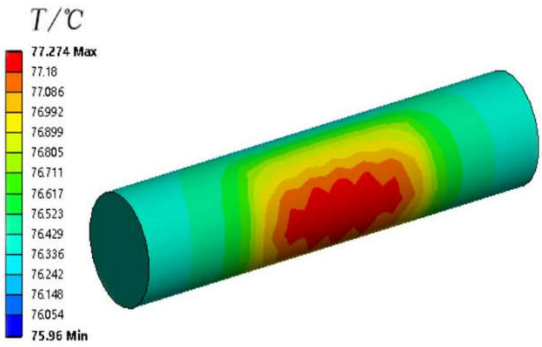

(f) Temperature rise of shaft

Preprints.org (www.preprints.org) | NOT PEER-REVIEWED | Posted: 7 May 2024 doi:10.20944/preprints202405.0341.v1

Figure 11. Temperature rise of each part of motor with non-uniform air gap structure at rated load for 120 min of operation.

In order to verify the correctness of the equivalent thermal network modeling and analysis results established in this paper, the analysis results of each component of the motor are compared with the average value of the simulation results, as shown in Table 2. It can be seen through the comparative analysis that the results of the equivalent thermal network method are basically the same as the simulation results, and the maximum error area exists in the armature winding, which is due to the long axial length of armature winding and the lower accuracy of the division using the equivalent thermal network method, as well as the faster heat transfer of the armature winding is made of copper. This is due to the fact that the armature winding has a long axial length, the equivalent thermal network method is less accurate, and the armature winding is made of copper, which transmits heat faster, so the average value of the calculation is more inaccurate.

Table 2. Average temperature rise at steady state for each motor component.

Component name	Equivalent thermal network method /℃	Simulation value of uniform air gap /℃	Simulation value of Non-uniform air gap/℃
Motor housing	84.6	90.5	82.5
Stator yoke	86.5	88.42	81.3
Armature winding	90.3	96.65	83.5
Stator teeth	91.8	93.75	80.5
SCPM	85.6	84.17	79.23
TRPM	83.5	84.27	77.32
Rotor core	82.1	83.71	76.85
RRPM	81.8	82.76	79.78
Shaft	77.8	79.68	76.56

6. Experimental Validation

In order to verify the validity of the established eddy current loss model of ITRPMM and the accuracy of the calculation results of the bidirectional magneto-thermal coupling method, two prototypes are test-fabricated respectively. Other things being equal, the experimental results of the permanent magnet motor are compared and analyzed for rotor eccentricity of 0mm and 4mm. The results are shown in Figure 12(a) and (b). And the PT100 thermistor is pre-buried at the end of the armature winding and in the stator slot of the motor to build the test platform of the interior non-uniform air-gap combined pole PM motor, as shown in Figure 12 (e).

(a) Uniform air gap rotor structure

(b) Non-uniform air gap rotor structure

Preprints.org (www.preprints.org) | NOT PEER-REVIEWED | Posted: 7 May 2024 doi:10.20944/preprints202405.0341.v1

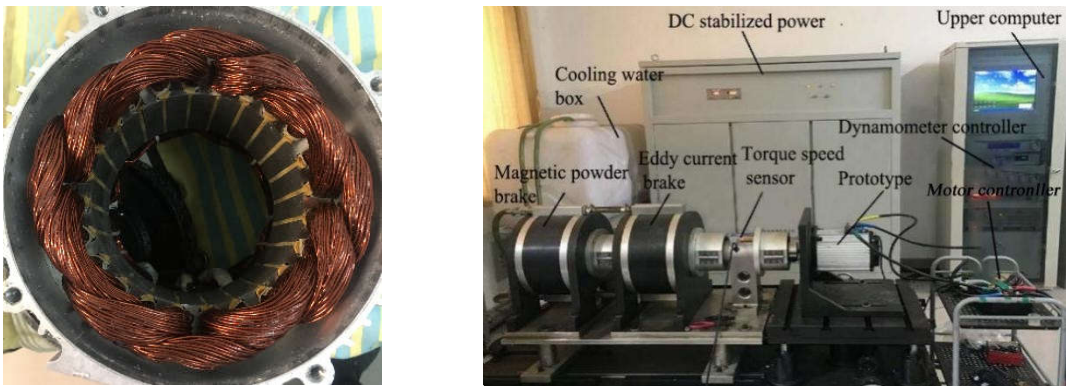

(c) Stator and armature winding (e) The diagram of test platform

Figure 12. Prototype and temperature rise experiment platform.

The temperature rise test of prototype using a thermal imager at 3 000 r/min is shown in Figure 13, and the steady state temperature cloud diagram of the prototype is shown in Figure 14. The maximum temperature of the motor housing is 89.5 ℃ , when the temperature rise is stable, and the maximum temperature rise of the motor housing is 90.747 ℃ in the bi-directional magnetic thermal coupling simulation results, and the simulation results are in good agreement with the experimental results, which proves the accuracy of the bi-directional magneto thermal coupling.

Figure 13. Thermal imaging camera.

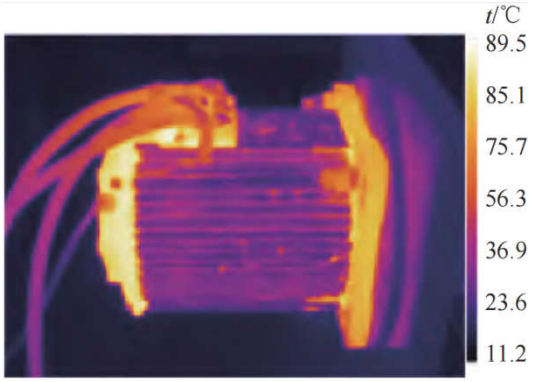

Figure 14. Steady state temperature cloud.

Through the motor temperature test experiment, the motor temperature rise test curve can be obtained as shown in Figure 15. When the uniform air gap permanent magnet motor runs for 120 min in no-load condition, the test value of stator winding temperature tends to steady state is 54℃, and the steady state temperature test value in rated load condition is 96℃. When the non-uniform air-gap PM motor is run for 120 min at no load, the steady-state temperature test value is 52°C, and the steady-state temperature test value at rated load condition is 89°C, which is consistent with the

Preprints.org (www.preprints.org) | NOT PEER-REVIEWED | Posted: 7 May 2024 doi:10.20944/preprints202405.0341.v1

theoretical calculations as well as the simulation results. The experimental results show that the permanent magnet motor with non-uniform air-gap rotor structure can effectively reduce the temperature rise of the armature winding, and the temperature difference between the non-uniform air-gap permanent magnet motor and the uniform air-gap permanent magnet motor is larger under the rated load condition, which verifies the correctness of the magneto-thermal bidirectional three-dimensional coupling model.

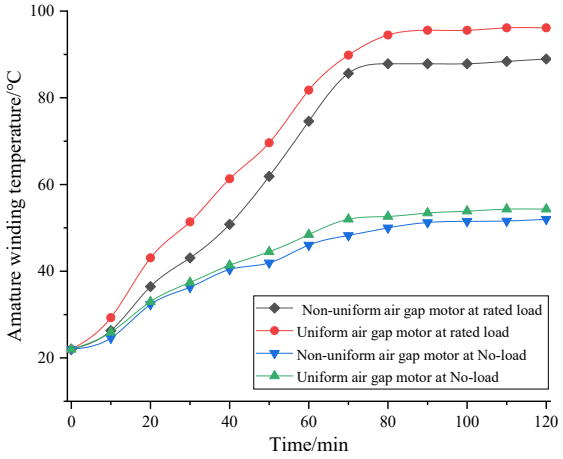

Figure 15. Maximum temperature rise contrast curve of armature winding.

In this paper, the no-load back electromotive force (EMF) test is carried out on the prototype by using the two-machine towing feedback method. The experimental platform of the prototype built is shown in Figure 16. For the experimental test, a permanent magnet motor with a rated power of 5kW, rated voltage of 72V, and rated speed of 3000r/min is used as a pilot motor, and the operating frequency and synchronous speed of the pilot motor are the same as those of the test motor.

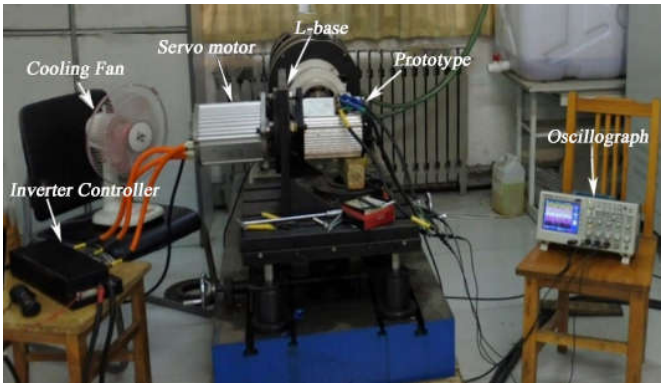

Figure 16. Experimental platform of no-load back EMF.

Under the rated speed, the waveform of no-load back electromotive force measured by the two prototypes ares shown in the Figure 17. It can be seen from the figure that when the motor is non-uniform air gap, the waveform of the back EMF is more similar to the sine law, and the waveform has a smoother curve, indicating that when the rotor eccentricity is 4mm, the high order harmonic content in magnetic density of air gap is less, thus verifying the correctness of the theoretical analysis method. When the air gap is uniform, the amplitude of no-load back EMF is 48V, and when the air gap is non-uniform, the amplitude of no-load back EMF is 51V. It can be seen that the design of non-uniform air gap is beneficial to enhance the amplitude of back EMF, because the design of non-uniform air gap improves peak value of air gap magnetic density of the motor when other conditions remain unchanged.

Preprints.org (www.preprints.org) | NOT PEER-REVIEWED | Posted: 7 May 2024 doi:10.20944/preprints202405.0341.v1

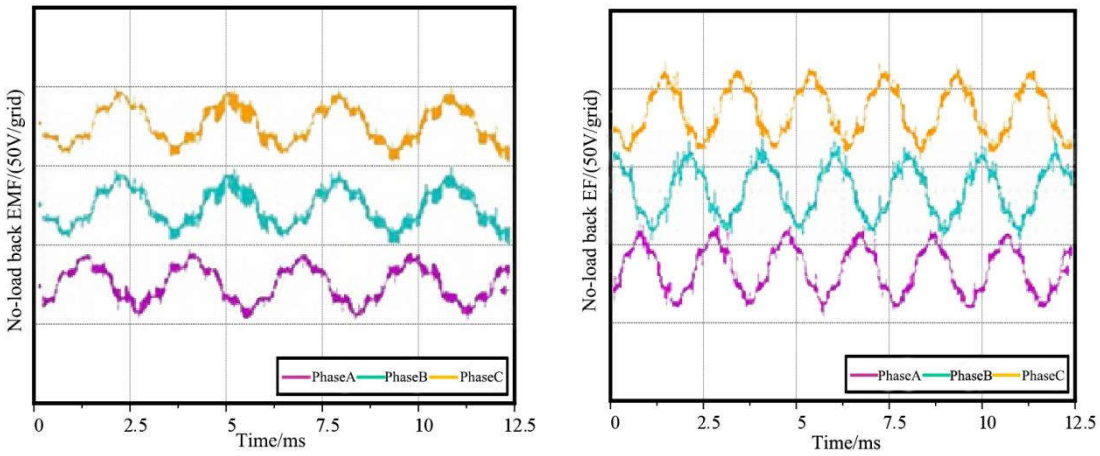

(a)No-load back EMF waveform with uniform airgap

(b) No-load back EMF waveform with non-uniform airgap

Figure 17. Measured waveform of no-load back EMF of prototype at rated speed.

7. Conclusion

(1) This paper proposes a new type of interior combined pole permanent magnet motor for electric vehicles. Through the establishment of the sinusoidal subdomain model of non-uniform air gap distribution and eddy current loss model, the analytical expression between rotor eccentricity and eddy current loss is derived, and it is calculated that when ITRPMM rotor eccentricity is 4mm, the waveform of the back EMF is more similar to sine. The content of higher harmonics in the air gap is the least and the eddy current loss is the least.

(2) The equivalent thermal network model of ITRPMM is established, and the temperature rise matrix expression of ITRPMM is obtained, and the temperature rise of each node of the motor is calculated. The finite element simulation of uniform air gap permanent magnet motor and non-uniform air gap permanent magnet motor is verified by magnetothermal bidirectional coupling method. It can be seen that when the permanent magnet motor adopts non-uniform air gap structure, the temperature rise of each component is significantly reduced. The calculation results of the equivalent thermal network method are between the simulation results of the uniform air gap permanent magnet motor and the non-uniform air gap permanent magnet motor, and the armature winding is the component with the largest error in the calculation results of the analytical method and the finite element method

(3) The prototype experiment shows that the permanent magnet motor with non-uniform air gap structure can effectively reduce the rotor eddy current loss and reduce the motor temperature rise, which is conducive to improving the power density of the motor, and is more suitable for permanent magnet drive motor for electric vehicles.

Author Contributions: Methodology, S.M.; Software, S.M. and K.C.; Validation, S.M. and C.L.; Formal analysis, C.L.; Data curation, K.C.; Writing—original draft, S.M. and C.L.; Writing—review and editing, C.L. and S.M.; Supervision, S.M. All authors have read and agreed to the published version of the manuscript.

Funding: This research was funded by National Natural Science Foundation of China (Grant number:52305276), Tianjin Education Commission Research Program Project (Grant number: 2022KJ122), Tianjin University of Technology and Education Scientific Research Project (Grant number: KYQD202339). I have carefully checked and found that the information of the fund is accurate and accurate

Data Availability Statement: The data presented in this study are available on request from the corresponding author. The data are not publicly available because they are part of ongoing research.

Conflicts of Interest: The authors declare no conflict of interest.

Preprints.org (www.preprints.org) | NOT PEER-REVIEWED | Posted: 7 May 2024 doi:10.20944/preprints202405.0341.v1

References

1. LIU Xiangdong, CHEN Hao, ZHAO Jing, et al. Research on the performances and parameters of interior PMSM used for electric vehicles [J]. IEEE Transactions on Industrial Electronics, 2016, 63(6): 3533–3545.
2. KOU Baoquan, ZHAO Xiaokun, ZHANG Haoquan, et al. Review and analysis of electromagnetic structure and magnetic field regulation technology of the permanent magnet synchronous motor [J]. Proceedings of the CSEE, 2021, 41(20): 7126–7141.
3. LI Xiang, KAN Chaohao, REN Taian, et al. Thermal network modeling and thermal stress evaluation for a high-power linear ultrasonic motor [J]. IEEE Transactions on Industry Applications, 2022, 58(6): 7181–7191.
4. LIN Mingyao, LE Wei, LIN Keman, et al. Overview on research and development of thermal design methods of axial flux permanent magnet machines [J]. Proceedings of the CSEE, 2021, 41(6): 1914–1929.
5. Dajaku G, Xie Wei, Gerling D. Reduction of low space harmonics for the fractional slot concentrated windings using a novel stator design[J]. IEEE Transactions on Magnetics, 2014, 50(5): 1-12.
6. HWANG S W, RYU J Y, CHIN J W, et al. Coupled electromagnetic-thermal analysis for predicting traction motor characteristics according to electric vehicle driving cycle [J]. IEEE Transactions on Vehicular Technology, 2021, 70(5):4262–4272.
7. KOU Baoquan, ZHAO Xiaokun, ZHANG Haoquan, et al. Review and analysis of electromagnetic structure and magnetic field regulation technology of the permanent magnet synchronous motor [J]. Proceedings of the CSEE, 2021, 41(20): 7126–7141.
8. LIU Xiaping,ZHU Zhiguo,CHEN Dong,et al. Analysis and experimental study of eddy current loss in axial flux permanent magnet motor based on rotor permanent magnet segment optimisation[J/OL]. Journal of Electrotechnology,1-15[2024-04-26].https://doi.org/10.19595/j.cnki.1000-6753.tces.230671.
9. Chen Q, Liang D, Jia S, et al. Analysis of multi-phase and multi-layer factional-slot concentrated-winding on pm eddy current loss considering axial segmentation and load operation[J]. IEEE Transactions on Magnetics, 2018, 54(11): 1-6.
10. Dajaku G, Gerling D. Eddy current loss minimization in rotor magnets of PM machines using high-efficiency 12-teeth/10-slots winding topology[C]// 2011 International Conference on Electrical Machines and Systems, Beijing, 2011: 1-6.
11. Dajaku G, Xie Wei, Gerling D. Reduction of low space harmonics for the fractional slot concentrated windings using a novel stator design[J]. IEEE Transa- ctions on Magnetics, 2014, 50(5): 1-12.
12. CHEN Zhenfei,XING Ning,MA Hongzhong,et al. Modelling and analysis of harmonic eddy current losses in permanent magnets of fractional slot permanent magnet motors[J]. Journal of Electrotechnology,2022,37(14):3514-3527.DOI:10.19595/j.cnki.1000-6753.tces.210112.
13. BENLAMINE R, DUBAS F, RANDI S A, et al. 3-D numerical hybrid method for PM eddy-current losses calculation : application to axial-flux PMSMs[J]. IEEE Transactions on Magnetics, 2015, 51(7) : 8106110.
14. Tong Wen-ming, Hou Mingjun, Sun Lu, et al. Analysis Method of Rotor Eddy Current Loss of High Speed permanent magnet Motor with retaining sleeveed rotor based on precise subdomain Model [J]. Transactions of China Electrotechnical Society, 2022,37 (16):4047-4059.
15. SHI Yanwen, WANG Jiabin, WANG Bo. Transient 3-D lumped parameter and 3-D FE thermal models of a PMASynRM under fault conditions with asymmetric temperature distribution [J]. IEEE Transactions on Industrial Electronics, 2021, 68(6):4623–4633.
16. DING Shuye, JIANG Xin, ZHU Min, et al. Starting and steady temperature rise investigation for permanent magnet synchronous motor based on lumped-parameter thermal-network [J]. Electric Machines and Control, 2020, 24(5): 143–150.
17. HWANG S W, RYU J Y, CHIN J W, et al. Coupled electromagnetic-thermal analysis for predicting traction motor characteristics according to electric vehicle driving cycle [J]. IEEE Transactions on Vehicular Technology, 2021, 70(5):4262–4272.
18. WANG Xiaoyuan, GAO Peng. Application of equivalent thermal network method and finite element method in temperature calculation of in-wheel motor [J]. Transactions of China Electrotechnical Society, 2016, 31(16): 26–33.

Disclaimer/Publisher's Note: The statements, opinions and data contained in all publications are solely those of the individual author(s) and contributor(s) and not of MDPI and/or the editor(s). MDPI and/or the editor(s) disclaim responsibility for any injury to people or property resulting from any ideas, methods, instructions or products referred to in the content.